Materials Modelling

Uğur Özhan Demli and Erdem Acar*

Design optimization of armored wheeled vehicle suspension lower control arm

https://doi.org/10.1515/mt-2021-2154

Abstract: In this study, design optimization of the lower control arm, one of the main parts of double wishbone system widely used in the armored wheeled vehicles, is performed. The crucial factor in design is to keep the vehicle weight at a minimum especially for the amphibious vehicles that can operate in both the land and water. In this study, after the validation of the finite element (FE) analysis of suspension lower control arm with on-vehicle tests, weight optimization study is performed by using surrogate models. In FE model validation, strain values are collected with strain-gauge from the lower control arm of the 8×8 wheeled vehicle and the similar boundary conditions are applied to the FE model. A surrogate based approach is used in optimization. The training points for surrogate models are generated by using central composite design. Genetic aggregation surrogate modelling technique available in ANSYS Workbench. It is found that the weight of the control arm can be reduced from 25.2 to 21.8 kg, indicating a weight reduction of 13.3%. This leads to approximately 27 kg weight reduction in total for 8×8 vehicle. Finally, the performance of the optimized design is evaluated under two off-design quasi-static load scenarios (pothole strike and pavement crushing) that may be exposed on the suspension while the vehicle is in motion and preferred by vehicle manufacturers. It is observed that obtained stress values are below the yield strength of the material, and the off design performance of the control arm is verified with the safety factor of 1.46 for pothole strike scenario, and 1.08 for pavement crushing.

Keywords: armored wheeled vehicle; experimental validation; finite element method; suspension control arm; weight optimization.

***Corresponding author: Erdem Acar**, Mechanical Engineering, TOBB University of Economics and Technology, Ankara, 06810, Turkey, E-mail: erdem.acar@gmail.com. https://orcid.org/0000-0002-3661-5563
Uğur Özhan Demli, Mechanical Engineering, TOBB University of Economics and Technology, Ankara, 06810, Turkey

1 Introduction

Over the last couple of decades, the importance of structural optimization in defense and automotive industries has been increased gradually. Suspension system is one of the most important subsystem of armored wheeled vehicles. Vehicle suspension system is a subsystem responsible for the safety and driving comfort of the vehicle since it carries the weight of whole body. The main tasks are to prevent road shocks to transmit the vehicle chassis and other components and to ensure vehicle stabilization, safety and comfort. Double wishbone suspension system, which is one of the independent suspension system designs in wheeled vehicles, has lower and uppers control arms. The general function of the control arms is to prevent the wheels from moving uncontrollably in all road conditions by forming the connection between suspension and the vehicle chassis. The lower control arm which is the main example problem of this study is found in every single suspension cell of the armored wheeled vehicles. The manufacture costs of arms cover a significant part of the total cost of this system. In this study, it is aimed to create a finite element (FE) model of the initial design of the vehicle suspension lower control arm, to verify this model with tests on vehicle and to make weight optimization by using surrogate models.

Design optimization of vehicle suspension systems has been conducted in various studies. While some of these studies are limited only to numerical analyses without any experimental ingredient, there also exist studies where the performances of the optimized designs are validated through tests. For instance, Solanki et al. [1] performed reliability-based design optimization of control arm of Corvette while making use of a multiscale material model in the structural analysis. Similarly, Song et al. [2] presented a case study of surrogate based optimization of a control arm, where weight reduction studies were conducted by using Kriging and response surface surrogate models. Viqaruddin and Reddy [3] performed weight reduction and stiffness improvement of a control arm based on static analysis and torsion analysis performed by using Radioss software. Yıldız et al. [4] used butterfly optimization algorithm for optimum shape design of automobile suspension components, where Kriging surrogate models were integrated into optimization. Karadere et al. [5] performed lightweight design of automobile suspension components using topology and shape optimization techniques. Balkan et al. [6] obtained optimum design of an air suspension seat using recent structural optimization techniques, where ECE R14 seat belt pulling test was simulated on the optimum design obtained, but no physical tests were conducted. Albak et al. [7] enhanced the design of a twist beam suspension system using population-based optimization techniques. In none of these aforementioned studies, structural tests at either subsystem or system level were performed.

Design optimization studies accompanied with structural testing include the following studies. Khode et al. [8] optimized the lower control arm suspension system in a light commercial vehicle (LCV). CATIA software was used for CAD modeling and ANSYS software was used for FE analysis. To identify and validate the stress values of existing LCV, a suitable fixture was designed and manufactured, and the control arm is mounted on a universal tester with LCV. Note that the experimental validation was performed at the component level in that study. Yende et al. [9] used topology optimization to remove the excess weight of the lower control arm of the Mac–Pherson suspension system. In that study, the FE model for initial design of the control arm has not been validated with the physical test, whereas the optimized design control arm directly manufactured and compared to FE model outputs by performing the test on universal testing machine. The experimental validation was performed at the component level. Gutiérrez–Moizant et al. [10] improved the design of a crank arm, where the FE results are compared to experimental test outputs. The measurements obtained in that study are collected by using rectangular strain gauge rosettes. All the test studies were performed at the component level by using a universal dynamic test bench. In all of these aforementioned studies, structural test conducted for experimental validation were performed at component level (i.e., subsystem level).

In this study, design optimization of a suspension lower control arm of 8 × 8 armored wheeled vehicle is performed, where the FE model of the initial design is validated through the measurements taken with a strain gauge on a "complete vehicle in the field." That is, different from the existing studies in the literature where subsystem level tests were conducted, structural tests at system-level are conducted in this study, providing a level of novelty compared to the existing studies in the literature.

The remainder of the paper is organized as follows. The problem definition of the optimization of the lower control arm for minimum weight is presented in Section 2. Finite element modeling and its validation process are detailed in Section 3. Surrogate based optimization details are given in Section 4. The optimization results are presented in Section 5. Additional off-design condition analysis on optimized model is explored in Section 6. Finally, the conclusion comments are given in Section 7.

2 Definition

The part discussed in this study is the lower control arm, which is one of the largest parts in the suspension system of an 8×8 wheeled armored military vehicle. The lower control arm is connected to the frame on the vehicle chassis by revolute joints from two different points, and on the wheel side, it is connected to the lower region of the knuckle holding the wheel end with a ball joint. The main task of the control arms is to prevent the uncontrolled movement of the wheels except for the up and down (along vertical axis direction) in any road condition the vehicle enters and to allow each suspension cell to function independently. The isometric view of the initial design is shown in Figure 1.

In this study, starting from an existing design, the control arm design optimization problem is formulated as given in Equations (1)–(4), seeking for minimum weight such that the maximum von Mises stress developed in the optimized control arm design should not exceed the maximum von Mises stress developed in the initial control arm design.

$$\text{Find } \mathbf{x} = \{d_1, d_2, d_3, d_4\} \tag{1}$$

$$\text{Minimize } W(\mathbf{x}) \tag{2}$$

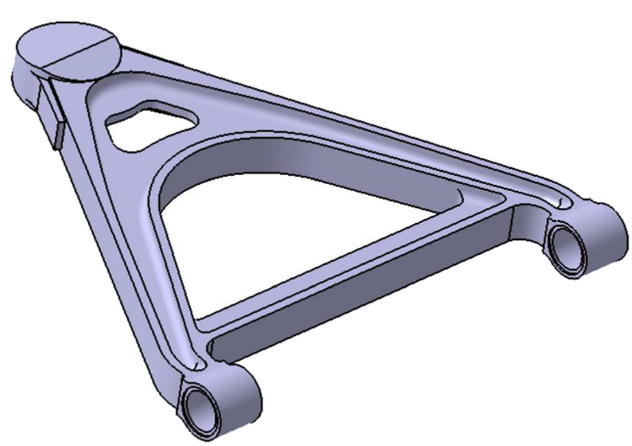

Figure 1: Isometric view of initial design of lower control arm.

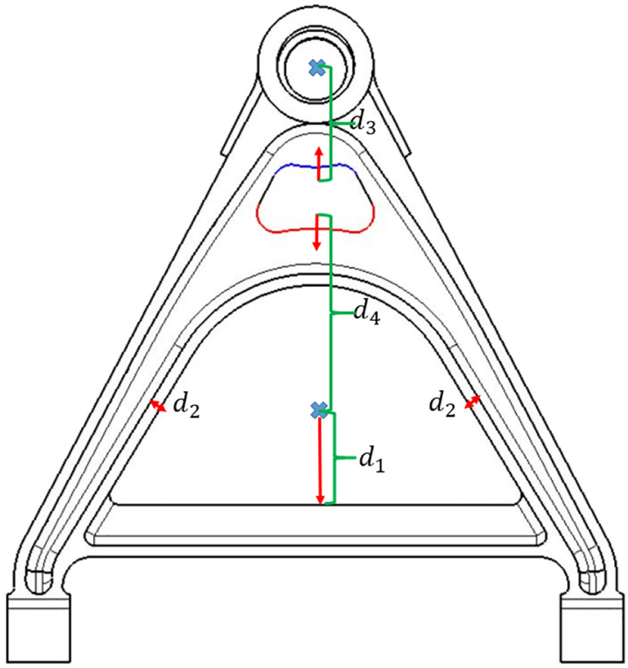

Figure 2: Design variables for the control arm.

$$\text{Subject to;}\ \sigma_{\text{MaxVM}}(\mathbf{x}) - \sigma^{\text{ini}}_{\text{MaxVM}} \le 0 \quad (3)$$

$$\mathbf{x}_{\text{L}} \le \mathbf{x} \le \mathbf{x}_{\text{U}} \quad (4)$$

The terms d_1, d_2, d_3, and d_4 given in Equation (1) represent the design variables and constitute the design variable vector **x**. These design variables change the shape of the control arm as shown in Figure 2. W(**x**) in Equation (2) is the weight of the control arm. The term $\sigma_{\text{MaxVM}}(\mathbf{x})$ represents the maximum von Mises stress developed in the control arm for a given design variable vector **x**, and the term $\sigma^{\text{ini}}_{\text{MaxVM}}$ is the maximum von Mises stress developed in the initial control arm design. Considering the dimensional constraints that should not be violated on the control arm, the design variables are limited with the lower limits $\mathbf{x}_{\mathbf{L}}$ and upper limits $\mathbf{x}_{\mathbf{U}}$ as given in Equation (4). The initial values of the design variables as well as their lower and upper limits are shown in Table 1.

Suspension control arms of the military vehicles are generally made cast steel or cast iron materials due to their high strength properties [11]. The material of the part considered in this study is austempered ductile cast iron with the properties given in Table 2.

Table 1: The initial values of the design variables as well as their lower and upper limits.

Design variables	Initial values	Lower limit	Upper limit
d_1 [mm]	75	75	105
d_2 [mm]	12	7	12
d_3 [mm]	103.9	80	103.9
d_4 [mm]	214.5	180	214.5

Table 2: Material specifications for the austempered ductile cast iron.

Material specifications	Unit	Value
Density (ρ)	kg·m^{-3}	7200
Yield strength (σ_{ty})	MPa	700
Poisson's ratio (ν)	–	0.28
Young's modulus (E)	GPa	130

3 Finite element modeling and validation

In this section, loading and boundary conditions of the analysis model on the initial design are explained first. Then, the mesh convergency studies are discussed. Finally, FEA model validation by testing the initial design part on vehicle is explained. Finite element modeling is performed using ANSYS Workbench 19.2.

3.1 Loading and boundary conditions

The loading and boundary conditions are determined by selecting a vehicle scenario for the analysis to be performed. The selected case reflects data obtained from the heaviest suspension cell with a mass of 4000 kg in the static and bump position, measured when the vehicle reaches the weighbridge.

The loading of the analysis models within the scope of the study are applied on the global model over the spindle in the schematic representation of the suspension cell in Figure 3. As explained in the problem definition section, the control arms are connected to the knuckle with ball joints and from the other end to the vehicle body by revolute joints. These boundary conditions have been preserved in all analyzes conducted within the scope of this study, and the analysis result images given belong to the submodel created under the global model. The connection points shown as body connection in the relevant model are assigned as the boundary condition in the ANSYS model as the revolute joint and the regions shown as the ball joint-knuckle connection as the spherical joint in the global model. In addition, similar links are also located on the upper control arm, while the upper point of the suspension unit is assigned as a fixed support in the global model.

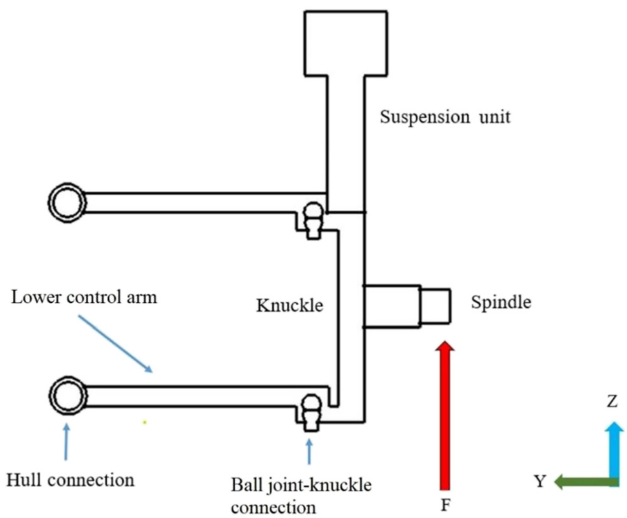

Figure 3: Schematic illustration of the global model of the suspension cell.

As a result of the 4000 kg load applied from the wheel, the reaction forces at two different points where the lower control arm is attached to the body are also shown. Figure 4A shows the loadings of 4780 N in the +*Z* direction, 13977 N in the −*Y* direction, and 6437 N in the −*X* direction at the control arm left connection point. Similarly, Figure 4B shows the loadings of 4780 N in the +*Z* direction, 13977 N in the −*Y* direction, and 6437 N in the +*X* direction at the control arm right connection point. Finally, Figure 4C shows the coordinates of the both connection points.

3.2 Mesh convergence

In the meshing studies, 10-node tetrahedral elements are used as shown in Figure 5. To conduct a mesh convergence study, FE analyses are performed for different element sizes. The coordinate of the maximum stress is obtained as (−122, −221, −17), and the variation of the maximum von Mises stress with respect to element size is obtained as shown in Figure 6 and Table 3. It is seen that the convergence is achieved at 2.5 mm element size, and this element size will be used in the subsequent optimization studies in the paper. The stress distribution in the converged mesh is shown in Figure 7. For this initial design, the mass is 25.2 kg, and the maximum von Mises stress developed in the control arm is 97.80 MPa.

3.3 Validation through field tests

Following the verification of the finite element model through the convergence study, it is aimed to validate it by gathering measurements on the manufactured part through field tests. In this study, measurements are taken from a region where the maximum von Mises stress is developed according to the FE model. That is, estimation of the stress distribution on the part through FE is served as a guide for the physical test. Figure 8 shows the strain gauge device on the lower control arm mounted on the 8 × 8 vehicle suspension in the workshop.

Since the test is carried out on the vehicle, stabilizer legs are placed on the vehicle chassis in accordance with safety precautions, and the test is continued with only wheel load. Since this reduced the load on the lower suspension arm, it caused the readings to be relatively small. The gauge factor (gauge factor) of the strain gauge used in the test is 2.125 ± 0.5%.

The left front axle is lifted up (with the help of forklift) to three different heights, and the strain is measured. Figure 9 shows the strain measurements obtained from three different suspension heights. It is seen that the average strain values corresponding to these three different suspension heights are determined as 75, 65, and 50 microstrains, respectively. Note that the strain in the *y* direction (ε_{yy}) is measure in the tests (the reader is referred to Figure 7 for the *y*-direction). In addition, when the percent difference results reported in the validation studies in the literature that performed similar strain gauge

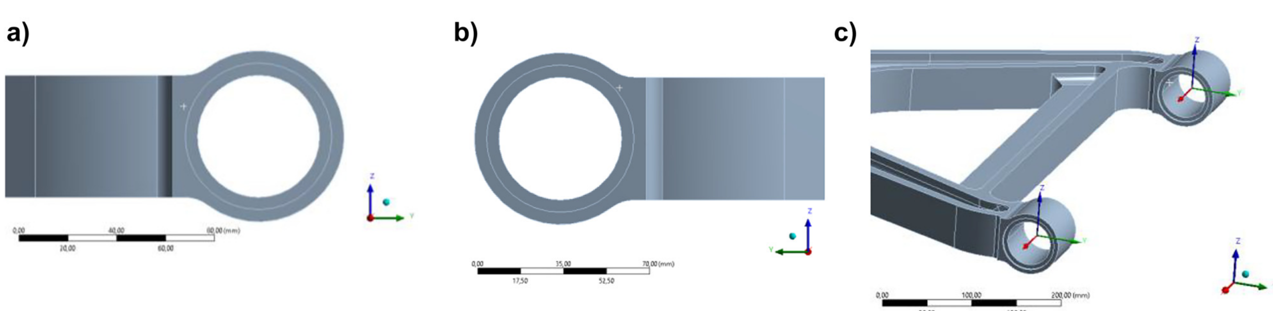

Figure 4: Control arm connection points, a) left, b) right, c) both.

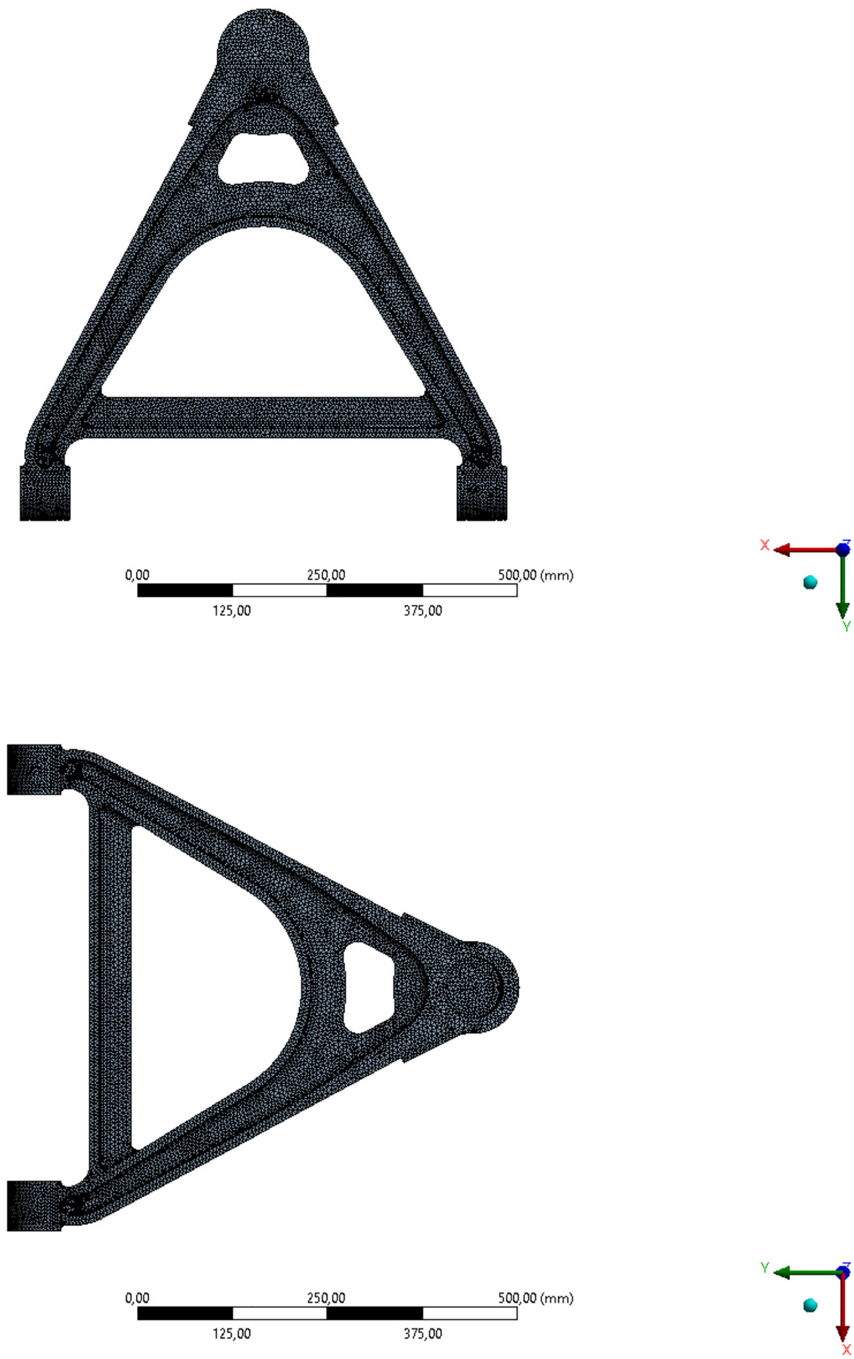

Figure 5: Finite element mesh of the control arm.

reading are examined, the results obtained in this study are considered to be suitable [10, 12, 13] (Table 4).

4 Surrogate based optimization

Since high-fidelity engineering simulations and analysis models require long periods of time and these analyzes are repeated many times during the design optimization, surrogate models are commonly used to reduce the computational cost. Surrogate model-based optimization studies generally and, respectively; include defining design space, experimental design studies, taking samples from experiments or simulations, creating surrogate models, and integrate them into an approximate optimization algorithm [14]. A typical flowchart for a surrogate-based optimization study is shown in Figure 10. At the beginning of design optimization, many design variables

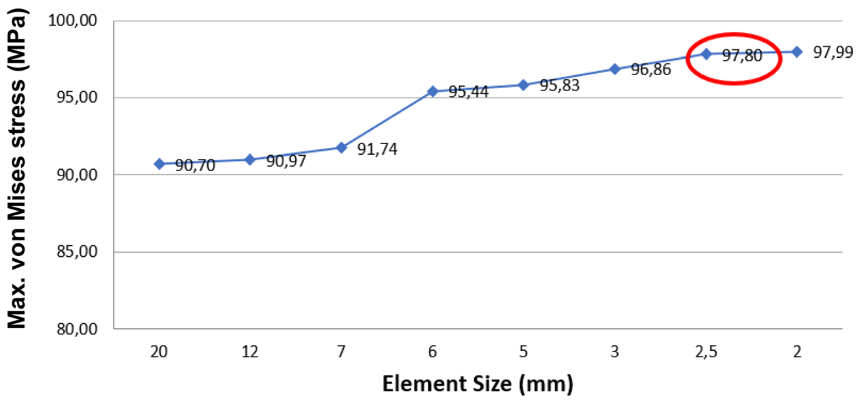

Figure 6: Mesh convergence results.

Table 3: Results of mesh convergence study.

Solution	Max. von Mises (MPa)	Element size (mm)	Number of nodes	Number of elements
1	90.70	20	396,403	286,073
2	90.97	12	461,350	330,716
3	91.74	7	506,755	355,183
4	95.44	6	593,717	414,799
5	95.83	5	670,586	464,850
6	96.86	3	1,478,833	1,015,083
7	97.80	2.5	2,103,918	1,449,267
8	97.99	2	3552,759	2,465,028

that are considered important are identified. However, since the large number of variables can increase the computational cost, less important variables can be eliminated by simplifying the design variables. This is done at the dimensionality reduction stage and can be determined by performing sensitivity analysis [15]. In order to evaluate different designs, after the generating the surrogate models, the main stages of which are shown, the search for the optimum design continues by using optimization algorithms (genetic algorithm, particle swarm optimization, simulated annealing, etc.) in the final stage. In this paper, the multi-objective genetic algorithm (MOGA), a variation of NSGA-II (Nondominated sorted genetic algorithm-II) based on a controlled elitist concept, available in ANSYS is used. MOGA determines the global optimum candidate points by working to optimize the objective functions until they converge to the maximum allowed pareto percentage by selection, crossover, and mutation [16].

Surrogate models are referred as meta-models, response surface models, auxiliary models, proxy models, or approximation models in the literature [17, 18]. The most commonly used surrogate methods include response surfaces [19], Kriging [20], radial based functions [21], nonparametric regression [22], artificial neural networks [23], and ensemble of surrogate models [24–26], which is termed as genetic aggregation in ANSYS. In this work, we use the genetic aggregation in ANSYS.

The training points for the surrogate models are generated by using the central composite design of experiments.

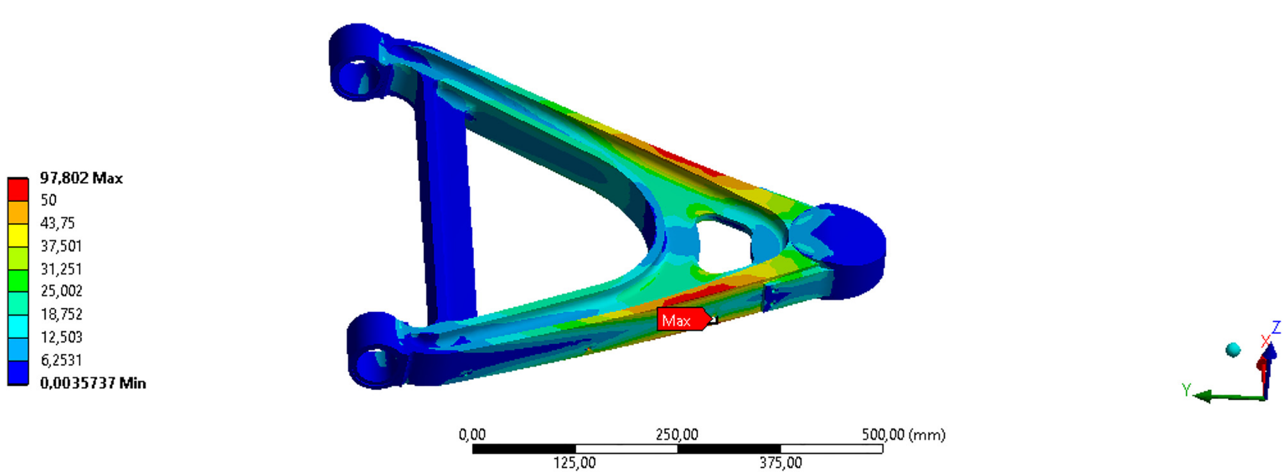

Figure 7: Von Mises stress (MPa) distribution in the initial design for the converged finite element model.

Figure 8: Strain gauge on the control arm.

Since we have four design variables, the central composite design formulation leads to $2^4 + 2\times4 + 1 = 25$ training points. The finite element analyses are performed for these training points, and the weight as well as the maximum von Mises stress values are calculated. Then, as noted earlier, genetic aggregation surrogate models available in ANSYS are constructed.

The accuracies of the constructed surrogate models are measured with root mean square error (RMSE), which expresses the root mean square of the errors (residuals). In this study, test points that are selected independently of the training points are used in RMSE calculation. It is a standard and popular error metric that can be applied to any surrogate model [20]. RMSE can be computed from

$$RMSE = \sqrt{\frac{1}{N}\sum_{i=1}^{N}\left(y_i - \hat{y}_i\right)^2} \tag{5}$$

with N: Number of test points, $\hat{y}_i$: Response prediction at the ith test point and y_i: Actual response at the ith test point.

Table 4: Comparison of field test and finite element analysis results.

No	Wheel force (N)	ε_{yy} predicted through FE model (micro m/m)	ε_{yy} measured in the test (micro m·m^{-1})	% difference
1	890	47.8	50.0	−4.4
2	1340	63.8	65.0	−1.9
3	1610	78.9	75.0	+5.2

In this study, five test points are generated. RMSE values for the mass as well as the maximum von Mises stress values are computed as 0.0259 kg and 2.59 MPa, respectively. We consider that RMSE for von Mises stress is prone to improvement (we shoot for RMSE less than 2 MPa), so we decide to further increase the accuracy of the surrogate models. When test points indicate that the response surface quality is poor or can be improved, these points can be used as refinement points to improve response surface quality. The refinement points are solved with a new simulation, as in the experimental design points, and new outputs are obtained and the response is used as input in surface generation. In addition, ANSYS DesignXplorer also allows the use of refinement points for surrogate model creation and validation, with the Universal Prediction-based Surrogate Modeling Adaptive Refinement Technique (UP SMART) algorithm [27].

There is an automatic refinement option specifically for the genetic aggregation solution. At least one of the result values (mass or von Mises stress value) must be selected for refinement. Here we select von Mises stress. The refinement points are then added to the training set to increase the response surface quality. In this second stage, five new test points are generated. Genetic aggregation surrogate models are re-constructed and the RMSE values are re-evaluated as 0.011 kg for mass, and 1.69 MPa for the

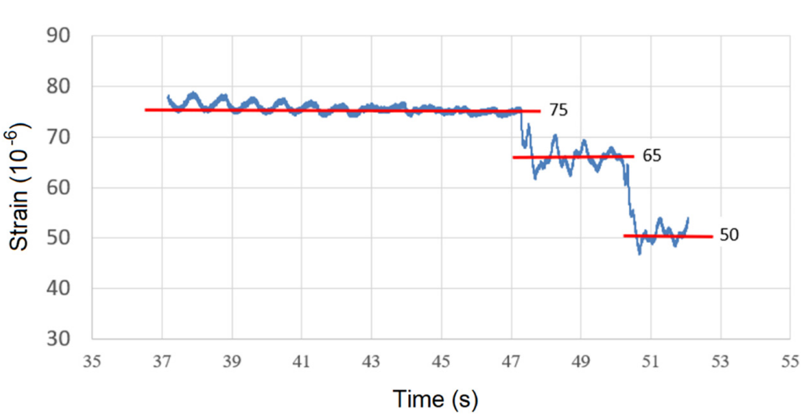

Figure 9: Strain gauge results corresponding to three different suspension heights.

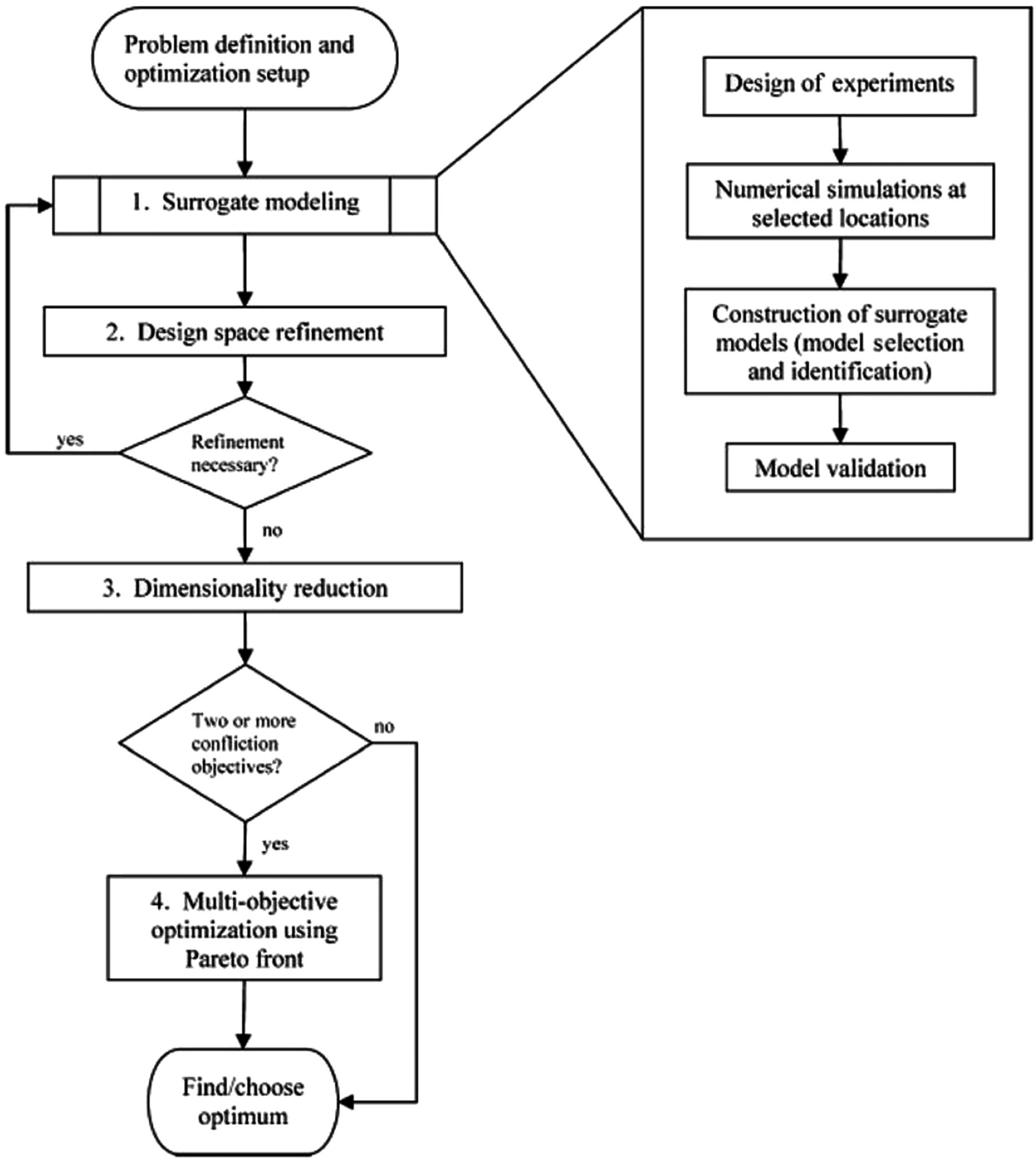

Figure 10: Surrogate based optimization flowchart [15].

maximum von Mises stress. We consider that the targeted RMSE values are achieved, so we terminate the improvement process. Finally, optimization problem stated earlier in Equation (1) is solved and the results are reported in the next section.

The training points constructed with central composite design of experiments (DoE) and the corresponding responses are listed in Table 5. The test points used to measure the accuracy of the surrogate models are given in Table 6. These test points are then used as refinement points in the next stage. The new test points in the next stage are given in Table 7.

5 Optimization

In the optimization step, multi-objective genetic algorithm (MOGA) method was used with ANSYS v19.2 software. The optimization results and comparison to initial design is given in Table 8. The initial weight of the lower control arm,

Table 5: Central composite DoE and the corresponding response.

No	d_1 (mm)	d_2 (mm)	d_3 (mm)	d_4 (mm)	Mass (kg)	Max. von Mises stress (MPa)
1	90.00	9.50	91.97	197.25	23.55	95.94
2	75.00	9.50	91.97	197.25	24.15	93.95
3	105.00	9.50	91.97	197.25	23.14	97.10
4	90.00	7.00	91.97	197.25	22.69	96.18
5	90.00	12.00	91.97	197.25	24.39	100.58
6	90.00	9.50	80.00	197.25	23.50	93.85
7	90.00	9.50	103.94	197.25	23.61	94.52
8	90.00	9.50	91.97	180.00	23.40	99.42
9	90.00	9.50	91.97	214.49	23.69	98.29
10	79.44	7.74	83.54	185.10	23.25	98.44
11	100.56	7.74	83.54	185.10	22.37	97.05
12	79.44	11.26	83.54	185.10	24.43	100.94
13	100.56	11.26	83.54	185.10	23.57	97.32
14	79.44	7.74	100.40	185.10	23.31	97.56
15	100.56	7.74	100.40	185.10	22.44	95.91
16	79.44	11.26	100.40	185.10	24.50	97.68
17	100.56	11.26	100.40	185.10	23.64	97.91
18	79.44	7.74	83.54	209.39	23.44	94.24
19	100.56	7.74	83.54	209.39	22.57	95.88
20	79.44	11.26	83.54	209.39	24.63	99.78
21	100.56	11.26	83.54	209.39	23.77	94.71
22	79.44	7.74	100.40	209.39	23.53	98.17
23	100.56	7.74	100.40	209.39	22.65	95.52
24	79.44	11.26	100.40	209.39	24.71	93.22
25	100.56	11.26	100.40	209.39	23.85	93.13

Table 6: Test points generated at the first stage.

No	d_1 (mm)	d_2 (mm)	d_3 (mm)	d_4 (mm)	Mass (kg)	Max. von Mises stress (MPa)
1	90.17	7.01	92.94	180.10	22.55	97.02
2	75.11	9.46	91.51	214.27	24.27	96.60
3	104.68	9.22	103.62	196.82	23.14	94.57
4	75.09	9.42	103.50	195.54	24.16	97.38
5	88.29	9.56	80.44	180.68	23.46	97.01

Table 7: Test points generated at the second stage.

No	d_1 (mm)	d_2 (mm)	d_3 (mm)	d_4 (mm)	Mass (kg)	Max. von Mises stress (MPa)
1	104.65	9.61	80.43	197.88	23.14	100.25
2	89.16	9.47	103.44	213.97	23.78	96.61
3	89.69	7.10	103.83	194.58	22.78	94.09
4	75.05	9.26	80.35	195.82	24.01	94.61
5	104.28	11.87	91.39	195.87	23.75	94.92

Table 8: Optimization results.

Design	d_1 (mm)	d_2 (mm)	d_3 (mm)	d_4 (mm)	Mass (kg)	Max. von Mises stress (MPa)
Initial	75.0	12.0	103.9	214.5	25.20	97.80
Optimum(pred.)[a]	105.0	7.0	80.7	180.3	21.87	96.67
Optimum(FE)[b]					21.85	97.03

[a]In optimum (pred.), the performance of the optimum is obtained from surrogate models. [b]In optimum (FE) the performance of the optimum is obtained from an additional FE run.

25.2 kg, decreased by 13.3% to 21.8 kg. This means that 3.35 kg per part and a total of approximately 27 kg reduction on the vehicle since there are 8 control arms on an 8×8 wheeled vehicle.

Furthermore, the fact that the maximum von Mises stress on the part did not increase after this weight reduction and a similar value was measured with a deviation of less than 1% means that the optimization was successful. Figure 11 shows the initial and optimum designs of the control arm, and Figure 12 shows the von Mises stress distribution in the optimum design.

6 Additional off-design condition analysis on optimized model

For the lower control arm whose weight optimization is just completed, analyses related to quasi-static critical road load scenarios (scenarios that can cause breakage and damage) are carried out in this section in order to examine the impact of different situations experienced during driving. The longitudinal impact describes the scenario in which the vehicle falls into a deep pothole while going straight. At the same time, lateral impact is the scenario that describes the vehicle wheel hitting a pavement at high speed or getting a hit directly on the lateral axis. Although it is considered that these scenarios will cause high damage to the suspension parts other than the control arms, it is expected that stress values will be obtained on the lower control arm, below the component yield strength value, as a result of the scenario. The safety factor for the results is also calculated. Selected two different road load scenarios are shown in Table 9. Based on these scenarios, the maximum von Mises stress values calculated on the lower control arm as a result of the loads applied on the wheel for both scenarios are given separately in Figures 13 and 14.

The results obtained according to the scenarios and the safety factors calculated based on these results are given in

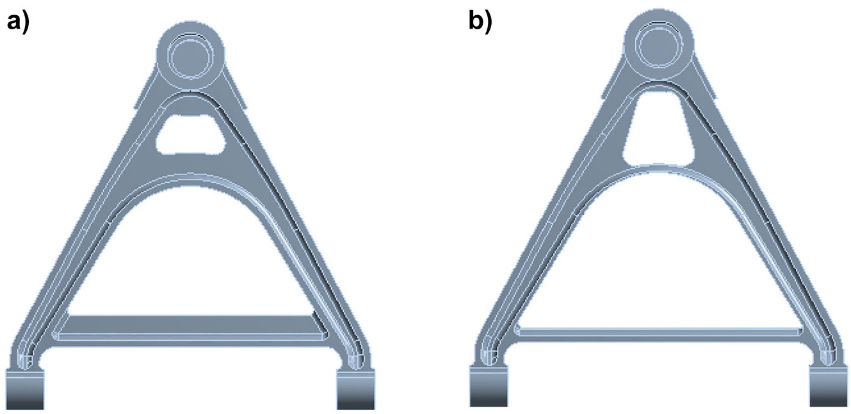

Figure 11: Design stages, a) initial design, b) optimum design.

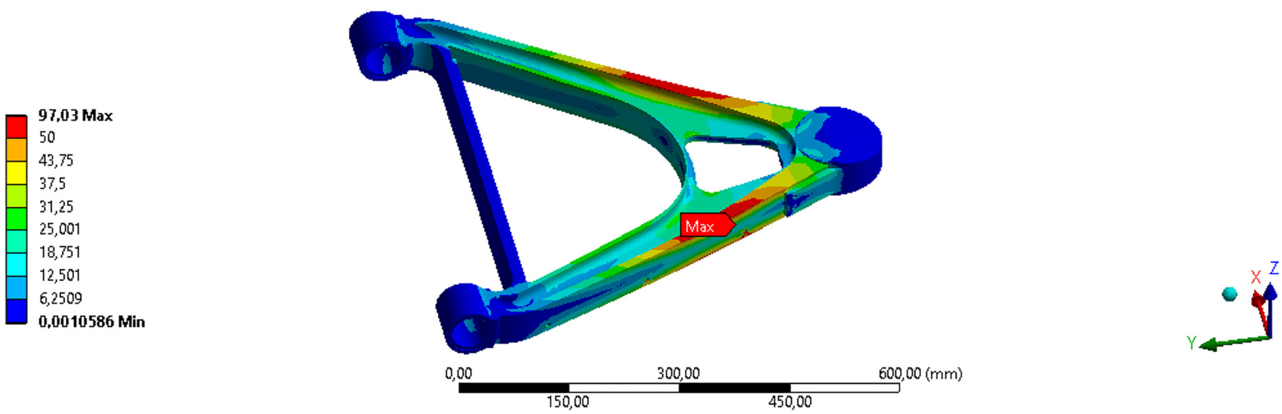

Figure 12: Von Mises stress (MPa) distribution in the optimum design.

Table 9: Road load off-design conditions.

	Road load scenarios	X (g)	Y (g)	Z (g)
1	Pothole strike (longitudinal impact)	2	0	3
2	Lateral strike (pavement crushing)	0	3	1

Table 10. Based on the results; it has been observed that the maximum von Mises stress value is below the yield strength of the part, resulting in a successful result and the effect of the lateral impact scenario on the control arm is greater than the other scenario. The reason for this is that the force applied to the wheel in the *Z* direction is primarily damped by the suspension shock absorbers and reflects less load on the control arms, however, it is observed that more load is placed on the control arm in lateral loads.

7 Conclusions

In this study, the lower control arm of the double wishbone suspension system of an 8×8 armored wheeled vehicle was optimized. The mass of the lower control arm, whose initial value was 25.2 kg, was reduced by 13.3% to 21.85 kg. There are 8 lower control arms in an 8×8 wheeled vehicle. This means that the total reduction of weight is approximately 27 kg for 1 vehicle. Vehicle weight is the most critical issue in land vehicles with high mobility and especially the ones have swimming requirement. The output of this study also contributes to weight reduction studies throughout the vehicle.

The optimized model was analyzed under two quasi-static load scenarios (off design conditions) and successful results were obtained by keeping the maximum von Mises stress under the part yield strength. The part was verified by finding the factor of safety 1.46 and 1.08.

The study discussed in this paper can be extended to the following studies:

- To perform optimized part validation in field, the part can be manufactured and subjected to life tests on an independent suspension test setup. This path is followed especially before the mass production of safety-critical parts.
- Off-design condition analysis can be extended by adding different scenarios separately such as destructive road loads when turning right or left.

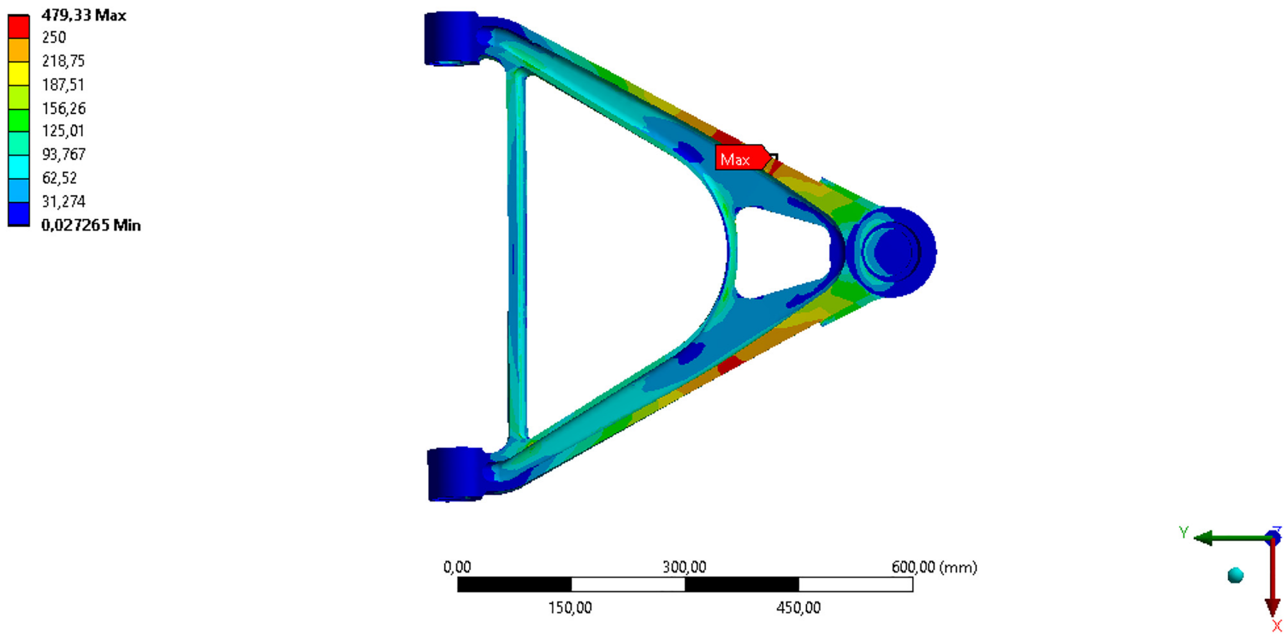

Figure 13: Von Mises stress (MPa) developed on the control arm as a result of the pothole strike scenario.

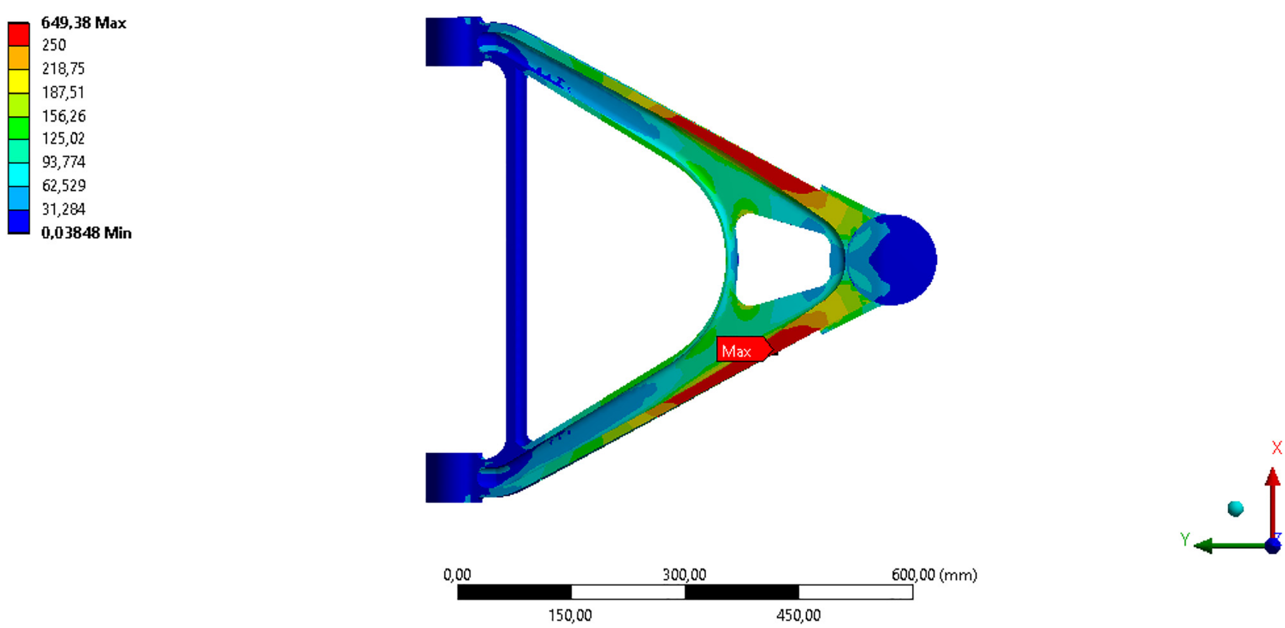

Figure 14: Von Mises stress (MPa) developed on the control arm as a result of the lateral strike scenario.

Table 10: FE analysis results of road load scenarios.

	Road load scenarios	Maximum von Mises (MPa)	Yield strength (MPa)	Safety factor
1	Pothole strike (longitudinal impact)	479.33	700	1.46
2	Lateral strike (pavement crushing)	649.38	700	1.08

Author contributions: All the authors have accepted responsibility for the entire content of this submitted manuscript and approved submission.

Research funding: None declared.

Conflict of interest statement: The authors declare no conflicts of interest regarding this article.

References

[1] K. N. Solanki, E. Acar, M. Rais-Rohani, M. Horstemeyer, and W. G. Steele, "Product design optimization with microstructure-property modeling and associated uncertainties," *Int. J. Des. Eng.*, vol. 2, no. 1, pp. 47–79, 2009, https://doi.org/10.1504/IJDE.2009.028446.

[2] X. G. Song, J. H. Jung, and H. J. Son, "Metamodel-based optimization of a control arm considering strength and durability performance," *Comput. Math. Appl.*, vol. 60, pp. 976–980, https://doi.org/10.1016/j.camwa.2010.03.019.

[3] M. Viqaruddin and D. R. Reddy, "Structural optimization of control arm for weight reduction and improved performance," *Mater. Today Proc.*, vol. 4, pp. 9230–9236, 2017, https://doi.org/10.1016/j.matpr.2017.07.282.

[4] B. S. Yıldız, A. R. Yıldız, E. İ. Albak, H. Abderazek, S. M. Sait, and S. Bureerat, "Butterfly optimization algorithm for optimum shape design of automobile suspension components," *Mater. Test.*, vol. 62, no. 4, pp. 365–370, 2020, https://doi.org/10.3139/120.111492.

[5] G. Karadere, Y. Düzcan, and A. R. Yıldız, "Light-weight design of automobile suspension components using topology and shape optimization techniques," *Mater. Test.*, vol. 62, no. 5, pp. 454–464, 2020, https://doi.org/10.3139/120.111492.

[6] A. Balkan, A. R. Yıldız, S. M. Sait, and S. Bureerat, "Optimum design of an air suspension seat using recent structural optimization techniques," *Mater. Test.*, vol. 62, no. 3, pp. 242–250, 2020, https://doi.org/10.3139/120.111477.

[7] E. İ. Albak, E. Solmaz, and F. Öztürk, "Enhancing a twist beam suspension system conceptual design using population-based optimization methods," *Mater. Test.*, vol. 62, no. 7, pp. 672–677, 2020, https://doi.org/10.3139/120.111532.

[8] S. Khode, A. Patil, and A. Gaikwad, "Design optimization of a lower control arm of suspension system in a LCV by using topological approach," *Int. J. Innovat. Res. Sci. Eng. Technol.*, vol. 6, no. 6, pp. 11657–11665, 2017.

[9] S. Yende, A. Tadamalle, and D. Burande, "Topology optimization of lower control arm for LMV," *Int. J. Mech. Eng. Res. Technol.*, vol. 8, no. 7, pp. 829–834, 2019.

[10] R. Gutiérrez-Moizant, M. Ramírez-Berasategui, J. A. Calvo, and C. Álvarez-Caldas, "Validation and improvement of a bicycle crank arm based on numerical simulation and uncertainty quantification," *Sensors*, vol. 20, no. 7, p. 1814, 2020, https://doi.org/10.3390/s20071814.

[11] P. A. Chacón, A. Sierra, and O. Gonzalez-Estrada, *Stress Analysis of a Suspension Control Arm*, Bucaramanga, Colombia, School of Mechanical Engineering, Universidad Industrial de Santander, Research report, 2018.

[12] L. F. Monaheng, W. B. Du Preez, A. Olwagen, and P. Haupt, "Strain gauge validation of finite element analysis of a TI6AL4V (ELI) mandibular implant produced through additive manufacturing," in *Conference Rapid Product Development Association of South Africa*, Gauteng, South Africa, Vaal University of Technology, 2016.

[13] E. Rahim, S. Shah, A. Dubov, "A preliminary biomechanical assessment of a polymer composite hip implant using an infrared thermography technique validated by strain gage measurements," *J. Biomech. Eng.*, vol. 133, no. 7, 2011, Art no. 074503, https://doi.org/10.1115/1.4004414.

[14] R. T. Haftka, Y. Zhang, N. Kim, "General-surrogate adaptive sampling using interquartile range for design space exploration," *J. Mech. Des.*, vol. 142, no. 5, 2020, Art no. 051402, https://doi.org/10.1115/1.4044432.

[15] Y. Mack, T. Goel, R. T. Haftka, and W. Shyy, "Surrogate model-based optimization framework: a case study in aerospace design," in *Evolutionary Computation in Dynamic and Uncertain Environments. Studies in Computational Intelligence*, vol. 51, S. Yang, Y. S. Ong, and Y. Jin, Eds., Berlin, Heidelberg, Springer, pp. 323–342.

[16] J. Wen and H. Yang, "Energy and cost optimization of shell and tube heat exchanger with helical baffles using Kriging metamodel based on MOGA," *Int. J. Heat Mass Transfer*, vol. 98, pp. 29–39, 2016, https://doi.org/10.1016/j.ijheatmasstransfer.2016.02.084.

[17] N. V. Queipo, R. T. Haftka, W. Shyy, T. Goel, R. Vaidyanathan, and P. K. Tucker, "Surrogate-based analysis and optimization," *Prog. Aero. Sci.*, vol. 41, no. 1, pp. 1–28, 2005, https://doi.org/10.1016/j.paerosci.2005.02.001.

[18] A. I. Forrester and A. J. Keane, "Recent advances in surrogate-based optimization," *Prog. Aero. Sci.*, vol. 45, nos. 1–3, pp. 50–79, 2009, https://doi.org/10.1016/j.paerosci.2008.11.001.

[19] R. H. Myers, D. C. Montgomery, and C. M. Anderson-Cook, *Response Surface Methodology: Process and Product Optimization Using Designed Experiments*, 4th ed., Hoboken, New Jersey, John Wiley & Sons, 2016.

[20] J. Sacks, W. J. Welch, T. J. Mitchell, and H. P. Wynn, "Design and analysis of computer experiments," *Stat. Sci.*, vol. 4, no. 4, pp. 409–423, 1989, https://doi.org/10.1214/ss/1177012413.

[21] N. Dyn, D. Levin, and S. Rippa, "Numerical procedures for surface fitting of scattered data by radial functions," *SIAM J. Sci. Stat. Comput.*, vol. 7, no. 2, pp. 639–659, 1986, https://doi.org/10.1137/0907043.

[22] W. Hardle, *Applied Nonparametric Regression*, New York, Cambridge University Press, 1990.

[23] C. M. Bishop, *Neural Networks for Pattern Recognition*, New York, Oxford University Press, 1995.

[24] E. Acar and M. Rais-Rohani, "Ensemble of metamodels with optimized weight factors," *Struct. Multidiscip. Optim.*, vol. 37, no. 3, pp. 279–294, 2009, https://doi.org/10.1007/s00158-008-0230-y.

[25] E. Acar, "Various approaches for constructing an ensemble of metamodels using local measures," *Struct. Multidiscip. Optim.*, vol. 42, no. 6, pp. 879–896, 2010, https://doi.org/10.1007/s00158-010-0520-z.

[26] M. B. Salem and L. Tomaso, "Automatic selection for general surrogate models," *Struct. Multidiscip. Optim.*, vol. 58, no. 2, pp. 719–734, 2018, https://doi.org/10.1007/s00158-018-1925-3.

[27] G. A. Banyay, S. D. Smith, and J. S. Young, "Sensitivity analysis of a nuclear reactor system finite element model," in *ASME Verification and Validation Symposium*, Minneapolis, MN, USA, May 16–18, 2018.

The authors of this contribution

Uğur Özhan Demli
Uğur Özhan Demli received his BSc and MSc degrees in Mechanical Engineering from TOBB University of Economics and Technology in 2016 and 2021, respectively. He works at the FNSS Savunma Sistemleri A.Ş. and his main fields of interests include structural design and optimization of wheeled and tracked armoured combat vehicles.

Erdem Acar
Dr. Erdem Acar is a professor in the Department of Mechanical Engineering, TOBB University of Economics and Technology, Ankara, Turkey. His research interests include optimization, design of automobile and aircraft structures, finite element analysis, ballistic simulations, and uncertainty analysis. He is an associate fellow of the American Institute of Aeronautics and Astronautics (AIAA) and he has been serving as a Review Editor for the journal of Structural and Multidisciplinary Optimization, Springer, since 2017.